15th Triennial World Congress, Barcelona, Spain

OPTIMAL MIXING BY FEEDBACK IN PIPE FLOW [1]

Ole Morten Aamo [*] **Andras Balogh** [**] **Miroslav Krstić** [**]

[*] *Department of Engineering Cybernetics, Norwegian University of Science and Technology, N–7491 Trondheim, Norway*
[**] *Department of MAE, University of California at San Diego, La Jolla, CA 92093–0411, USA*

Abstract: We design a Lyapunov based boundary feedback controller for achieving mixing in a 3D pipe flow governed by Navier-Stokes equations. We show that the control law maximizes a measure of mixing that incorporates stretching and folding of material elements, while at the same time minimizing the control effort and the sensing effort. The penalty on sensing results in a static *output*-feedback control law (rather than full-state feedback). We also derive a lower bound on the gain from the control effort to the mixing measure. Furthermore, we establish input/output-to-state-stability properties for the open-loop system. These results show a form of detectability of mixing in the interior of the pipe from the chosen outputs on the wall. The effectiveness of the optimal control in achieving mixing enhancement is demonstrated in numerical simulations.

Keywords: Nonlinear control systems, Lyapunov methods, Optimality

1. INTRODUCTION

Rigorous application of control systems theory to problems in mixing appeared for the first time in (D'Alessandro *et al.*, 1998; D'Alessandro *et al.*, 1999), and more recently in (Noack *et al.*, 2000). In (Aamo *et al.*, submitted), we applied active feedback control in order to enhance existing instability mechanisms in a 2D model of plane channel flow. By applying boundary control intelligently in a feedback loop, mixing was considerably enhanced with relatively small control effort. Wall-normal suction and blowing was used for actuation, and the pressure difference between opposite points on the wall for sensing. The control law was decentralized and designed using Lyapunov stability analysis.

In the current work, these efforts are successfully extended to 3D pipe flow, which, in the uncontrolled case, has a parabolic steady state solution (known as Hagen-Poiseuille flow). With mixing in mind, we quantify the flow perturbations (away from the Hagen-Poiseuille flow) in terms of the L_2-norm of their first order spatial derivatives. This norm is a volume integral over the entire flow domain. It explicitly incorporates stretching of material elements, and due to the boundedness of the domain, and the fact that the flow field satisfies the Navier-Stokes equations, folding is implicit in the measure. Since stretching and folding are key ingredients in mixing, the measure appears to be strongly related to mixing.

We design a Lyapunov based control law and show that it maximizes the measure of mixing described above, while at the same time minimizing the control effort and the sensing effort. The penalty on sensing results in a static *output*-feedback control law (rather than full-state feedback). We also derive a lower bound on the gain from the control effort to the mixing measure.

In separate results, we establish input/output-to-state-stability properties for the open-loop system. These results show a form of detectability of mixing in the interior of the pipe from the chosen outputs on the wall.

The effectiveness of the optimal control in achieving mixing enhancement is demonstrated in numerical simulations of the full, nonlinear, Navier-Stokes equations for 3D pipe flow at Reynolds number 2100. To quantify mixing, massless particles are placed into the flow, simulating passive tracer dye. Visualizations compare perturbation energy, enstrophy, vorticity, and dye distribution for the uncontrolled and controlled cases.

The feedback system designed in this work stands a good chance of being realizable, due to its simplicity: sensing and actuation are restricted to the pipe wall; and the feedback law is decentralized and static. Furthermore, simulations show that the spatial changes in the control velocity are smooth and small, promising that a low number of actuators will suffice in practice.

[1] This work was supported by the Norwegian Research Council, the Office of Naval Research, the Air Force Office of Scientific Research, and the National Science Foundation.

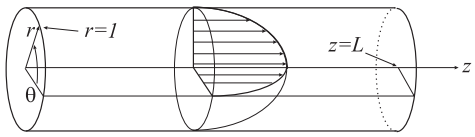

Fig. 1. Geometry of the pipe flow.

This paper is organized as follows: in Section 2 we present the governing equations; in Section 3 we introduce our choices of sensing and actuation; in Section 4 we define two measures of the fluid flow field which are instrumental to the theoretical analysis; in Section 5 we provide an energy analysis resulting in two technical lemmas that are frequently used in the analysis; in Section 6 we present the main result on control design and optimality; in Section 7 we discuss detectability of mixing, and finally; in Section 8 numerical simulations are presented.

2. NAVIER-STOKES EQUATIONS FOR 3D PIPE FLOW

The domain for the 3D pipe flow is the cylinder $\Omega = \{(r,\theta,z) \in [0,1) \times [0,2\pi) \times [0,L)\}$ (see Figure 1), on which the velocity field (V_r, V_θ, V_z) is defined. In the angular (θ) direction the boundary conditions are clearly periodic. In the streamwise (z) direction, we also use periodic boundary conditions. That is, we equate the flow quantities at $\theta = 0$ and $\theta = 2\pi$, and at $z = 0$ and $z = L$. In the radial direction (r) we impose the boundary conditions that the velocity be finite at $r = 0$, and at the wall $(r = 1)$ we will eventually specify the flow velocity as a boundary control law, but for now we use no-slip. Under these boundary conditions, one may verify that the velocity field

$$(\bar{V}_r, \bar{V}_\theta, \bar{V}_z, \bar{P}) = \left(0, 0, 1-r^2, -\frac{4}{Re}z\right) \qquad (1)$$

is a steady state solution (the Hagen-Poisuille flow) of the Navier-Stokes equations. Writing the Navier-Stokes equations in terms of perturbation variables, defined as

$$v_r \triangleq V_r,\ v_\theta \triangleq V_\theta,\ v_z \triangleq V_z - \bar{V}_z,\ \text{and}\ p \triangleq P - \bar{P},$$

we have

$$\begin{aligned}\frac{\partial v_r}{\partial t} + v_r\frac{\partial v_r}{\partial r} + \frac{v_\theta}{r}\frac{\partial v_r}{\partial \theta} - \frac{v_\theta^2}{r} + v_z\frac{\partial v_r}{\partial z} + \bar{V}_z\frac{\partial v_r}{\partial z} \\ = -\frac{\partial p}{\partial r} + \frac{1}{Re}\left(\frac{\partial}{\partial r}\left(\frac{1}{r}\frac{\partial}{\partial r}(rv_r)\right)\right. \\ \left. + \frac{1}{r^2}\frac{\partial^2 v_r}{\partial \theta^2} - \frac{2}{r^2}\frac{\partial v_\theta}{\partial \theta} + \frac{\partial^2 v_r}{\partial z^2}\right) \qquad (2)\end{aligned}$$

$$\begin{aligned}\frac{\partial v_\theta}{\partial t} + v_r\frac{\partial v_\theta}{\partial r} + \frac{v_\theta}{r}\frac{\partial v_\theta}{\partial \theta} + \frac{v_r v_\theta}{r} + v_z\frac{\partial v_\theta}{\partial z} + \bar{V}_z\frac{\partial v_\theta}{\partial z} \\ = -\frac{1}{r}\frac{\partial p}{\partial \theta} + \frac{1}{Re}\left(\frac{\partial}{\partial r}\left(\frac{1}{r}\frac{\partial}{\partial r}(rv_\theta)\right)\right. \\ \left. + \frac{1}{r^2}\frac{\partial^2 v_\theta}{\partial \theta^2} + \frac{2}{r^2}\frac{\partial v_r}{\partial \theta} + \frac{\partial^2 v_\theta}{\partial z^2}\right) \qquad (3)\end{aligned}$$

$$\begin{aligned}\frac{\partial v_z}{\partial t} + v_r\frac{\partial v_z}{\partial r} + v_r\frac{\partial \bar{V}_z}{\partial r} + \frac{v_\theta}{r}\frac{\partial v_z}{\partial \theta} + v_z\frac{\partial v_z}{\partial z} + \bar{V}_z\frac{\partial v_z}{\partial z} \\ = -\frac{\partial p}{\partial z} + \frac{1}{Re}\left(\frac{1}{r}\frac{\partial}{\partial r}\left(r\frac{\partial v_z}{\partial r}\right)\right. \\ \left. + \frac{1}{r^2}\frac{\partial^2 v_z}{\partial \theta^2} + \frac{\partial^2 v_z}{\partial z^2}\right) \qquad (4)\end{aligned}$$

$$\frac{1}{r}\frac{\partial}{\partial r}(rv_r) + \frac{1}{r}\frac{\partial v_\theta}{\partial \theta} + \frac{\partial v_z}{\partial z} = 0. \qquad (5)$$

3. SENSING AND ACTUATION

As mentioned in the previous section, the boundary conditions on the wall of the pipe incorporate our actuation. The fluid velocity at the wall is restricted to be normal to the wall, that is, we take v_{r-w} as the control input, and set $v_{\theta-w} = v_{z-w} = 0$, where we have defined, for notational convenience, the variables on the wall as

$$\begin{aligned}v_{r-w}(\theta,z,t) &\triangleq v_r(1,\theta,z,t),\\ v_{\theta-w}(\theta,z,t) &\triangleq v_\theta(1,\theta,z,t),\ \text{and}\\ v_{z-w}(\theta,z,t) &\triangleq v_z(1,\theta,z,t).\end{aligned}$$

We also impose on the control input that it satisfies

$$v_{r-w}(\theta,z,t) = -v_{r-w}(\theta+\pi,z,t), \qquad (6)$$

which states that if suction is applied at a point (θ,z) on the pipe wall, then an equal amount of blowing is applied at the opposite point $(\theta+\pi,z)$. It is clear that condition (6) ensures a zero net mass flux across the pipe wall, and therefore it is a natural condition to impose from a mass balance point of view. The measurement available is the pressure drop, denoted Δp, from any point (θ,z) on the pipe wall to the opposite point $(\theta+\pi,z)$. That is,

$$\Delta p(\theta,z,t) \triangleq p(1,\theta,z,t) - p(1,\theta+\pi,z,t). \qquad (7)$$

4. MEASURES OF MIXING

There are two key ingredients to effective mixing. The fluid flow field must inflict extensive stretching to material elements, and the stretching should be accompanied by folding. In this work, we define two measures of the fluid flow field that are instrumental to our development below. One is the kinetic energy of the perturbation, defined as

$$E(\mathbf{w}) \triangleq \frac{1}{2}\int_0^L\int_0^{2\pi}\int_0^1 (v_r^2 + v_\theta^2 + v_z^2)\, r dr d\theta dz, \qquad (8)$$

and the other is a measure of spatial velocity gradients, defined as

$$\begin{aligned}m(\mathbf{w}) \triangleq \int_0^L\int_0^{2\pi}\int_0^1 \left[\left(\frac{\partial v_r}{\partial z}\right)^2 + \left(\frac{\partial v_\theta}{\partial z}\right)^2\right. \\ \left. + \left(\frac{\partial v_z}{\partial r}\right)^2 + \left(\frac{1}{r}\frac{\partial v_z}{\partial \theta}\right)^2 + \left(\frac{\partial v_z}{\partial z}\right)^2\right.\end{aligned}$$

$$+\left(\frac{\partial v_r}{\partial r}\right)^2+\left(\frac{\partial v_\theta}{\partial r}\right)^2+\left(\frac{v_r}{r}+\frac{1}{r}\frac{\partial v_\theta}{\partial \theta}\right)^2 + \left(\frac{v_\theta}{r}-\frac{1}{r}\frac{\partial v_r}{\partial \theta}\right)^2\Bigg] r dr d\theta dz. \quad (9)$$

The latter measure, (9), appears to be stronger connected to mixing. While it is clear that stretching of material elements is explicit in a measure of spatial gradients of the flow field, folding is implicit in the measure due to the boundedness of the flow domain, and the fact that $\mathbf{w}$ satisfies the Navier-Stokes equations. Thus, our objective becomes that of designing a feedback control law, in terms of suction and blowing of fluid normally to the pipe wall, that is optimal with respect to some meaningful cost functional related to $m(\mathbf{w})$.

5. ENERGY ANALYSIS

Before giving the main result on controller design and optimality, we state two key lemmas that are needed frequently in what follows. The first lemma is a Lyapunov type result and it relates the time derivative of $E(\mathbf{w}(t))$ to $m(\mathbf{w}(t))$. The second lemma provides a bound on a crossterm in the streamwise (v_z) and radial (v_r) velocities, originating from the nonlinear convective terms in the Navier-Stokes equations. The proofs of the results presented in this paper can be found in (Balogh *et al.*, submitted).

Lemma 1. If $v_{\theta-w}$ and v_{z-w} are zero, and v_{r-w} satisfies (6), then

$$\dot{E}(\mathbf{w}) = -\frac{1}{Re}m(\mathbf{w}) - \frac{1}{2}\int_0^L\int_0^{2\pi} v_{r-w}\Delta p d\theta dz - \frac{1}{Re}\int_0^L\int_0^{2\pi} v_{r-w}^2 d\theta dz - \int_0^L\int_0^{2\pi}\int_0^1 r v_z v_r \frac{\partial \bar{V}_z}{\partial r} dr d\theta dz \quad (10)$$

along solutions of system (2)–(5).

Lemma 2. If v_{z-w} is zero, then solutions of system (2)–(5) satisfy

$$\int_0^L\int_0^{2\pi}\int_0^1 v_z v_r \frac{\partial \bar{V}_z}{\partial r} r dr d\theta dz \le \frac{a}{2}(1+b)\int_0^L\int_0^{2\pi} v_{r-w}^2 d\theta dz + \frac{a}{4}\left(1+\frac{1}{b}\right)\int_0^L\int_0^{2\pi}\int_0^1 \left(\frac{\partial v_r}{\partial r}\right)^2 r dr d\theta dz + \frac{1}{4a}\int_0^L\int_0^{2\pi}\int_0^1 \left(\frac{\partial v_z}{\partial r}\right)^2 r dr d\theta dz \quad (11)$$

for arbitrary positive constants a and b.

The conditions of Lemma 1 and 2 are assumed to hold throughout the analysis that follows, that is: $v_{\theta-w} = v_{z-w} = 0$, and; v_{r-w} satisfies (6).

6. OPTIMALITY

The following theorem incorporates the control design and optimality result.

Theorem 1. The control

$$v_{r-w} = -k\Delta p, \quad (12)$$

with $k \in \left(0, \frac{Re}{4}\right)$ and Re arbitrary, maximizes the cost functional

$$J(v_{r-w}) = \lim_{t\to\infty}\left[2\beta E(\mathbf{w}(t)) + \int_0^t h(\mathbf{w}(\tau))\, d\tau\right] \quad (13)$$

where

$$\beta = \frac{2k}{\left(1-\frac{4}{Re}k\right)}$$

and

$$h(\mathbf{w}) = \frac{2\beta}{Re}m(\mathbf{w}) + 2\beta\int_0^L\int_0^{2\pi}\int_0^1 v_z v_r \frac{\partial \bar{V}_z}{\partial r} r dr d\theta dz - \int_0^L\int_0^{2\pi} v_{r-w}^2 d\theta dz - \left(\frac{\beta}{2}\right)^2\left(1+\frac{2\beta}{Re}\right)^{-1}\int_0^L\int_0^{2\pi}\Delta p^2 d\theta dz. \quad (14)$$

Moreover, solutions of system (2)–(5) satisfy

$$h(\mathbf{w}) \le c_1 m(\mathbf{w}) - c_2\int_0^L\int_0^{2\pi}\Delta p^2 d\theta dz - \frac{1}{2}\int_0^L\int_0^{2\pi} v_{r-w}^2 d\theta dz \quad (15)$$

for arbitrary values of the control v_{r-w}, and with

$$c_1 = \frac{2\beta}{Re} + \max\left(\frac{1}{4}, 2\beta^2\right) > 0$$

$$c_2 = \left(\frac{\beta}{2}\right)^2\left(1+\frac{2\beta}{Re}\right)^{-1} > 0.$$

The objective of applying the control input (12) is to increase the value of $m(\mathbf{w})$. That this objective is targeted in the cost functional (13), is clear from inequality (15), which gives an upper bound on $h(\mathbf{w})$ in terms of $m(\mathbf{w})$. Thus, $h(\mathbf{w})$ cannot be made large without making $m(\mathbf{w})$ large, so the cost functional (13) is meaningful with respect to our objective. The cost functional also puts penalty on the output. Since the output is fed back to the control input, the output penalty works in conjunction with the input penalty to minimize control effort.

The next theorem writes the result of Theorem 1 on a form that puts emphasis on signal gains.

Theorem 2. For all Re and $t \geq 0$, solutions of system (2)–(5) satisfy

$$\max_{\substack{v_{r-w} \\ E(\mathbf{w}(0)) \neq 0}} \left\{ \lim_{t \to \infty} \frac{e(t) + \int_0^t g(\mathbf{w}(\tau))\, d\tau}{e(0) + \int_0^t b(\mathbf{w}(\tau))\, d\tau} \right\} = 1, \tag{16}$$

where

$$g(\mathbf{w}) \leq c_1 m(\mathbf{w}), \tag{17}$$

$$b(\mathbf{w}) \triangleq c_2 \int_0^L \int_0^{2\pi} \Delta p^2 d\theta dz + \frac{1}{2} \int_0^L \int_0^{2\pi} v_{r-w}^2 d\theta dz$$

and

$$e(t) \triangleq 2\beta E(\mathbf{w}(t)).$$

Furthermore, the maximum is achieved with the optimal control (12), for which solutions of the closed–loop system satisfy

$$2\beta E(\mathbf{w}(t)) + c_1 \int_0^t m(\mathbf{w}(\tau))\, d\tau \geq 2\beta E(\mathbf{w}(0)) + \left(\frac{3}{2} + \frac{2\beta}{Re}\right) \int_0^t \int_0^L \int_0^{2\pi} v_{r-w}^2 d\theta dz d\tau. \tag{18}$$

The result (16) was inspired by the work on optimal destabilization of linear systems reported by Mezić (2001). In view of (17), by maximizing the ratio in the curly brackets of (16), we make sure that the input and output signals are small compared to the internal states. This is equivalent to obtaining a large closed-loop gain. In addition, the theorem gives a lower bound on the states in terms of the control input for system (2)–(5) in closed loop with (12). Thus, it establishes the fact that the states cannot be small without the control input being small, and the control input cannot be made large without making the states large. As we shall see in our simulation study, this will lead to good mixing with low control effort.

7. DETECTABILITY OF MIXING

Achieving optimality with static output feedback of Δp is remarkable. In this section we explain why this special output is strongly related to mixing and allows its enhancement. The next theorem establishes an open-loop property of system (2)–(5) that is reminiscent of an integral variant of input/output-to-state-stability (IOSS) for finite dimensional nonlinear systems.

Theorem 3. If $Re \in (0, 4)$, then solutions of system (2)–(5) satisfy

$$c_3 \int_0^t m(\mathbf{w}(\tau))\, d\tau \leq 2\beta E(\mathbf{w}(0)) + \beta^2 \left(1 + \frac{2\beta}{Re}\right)^{-1} \int_0^t \int_0^L \int_0^{2\pi} \Delta p^2 d\theta dz d\tau + c_4 \int_0^t \int_0^L \int_0^{2\pi} v_{r-w}^2 d\theta dz d\tau, \tag{19}$$

for all $t \geq 0$ and for arbitrary values of the control v_{r-w}, with

$$c_3 = \frac{\beta}{4}\left(\frac{4 - Re}{Re}\right) > 0 \text{ and}$$
$$c_4 = 1 + \beta\left(\frac{4 + Re}{4 - Re}\right) > 0.$$

The significance of inequality (19) is that it provides a notion of detectability of internal states from the output Δp. In particular, if $m(\mathbf{w})$ is large, Δp must be large as well, or if Δp is small, so is $m(\mathbf{w})$. This is reminiscent of an integral variant of the IOSS property for finite-dimensional nonlinear systems, as defined by Krichman *et al.* (2001) (and motivated by earlier results in (Sontag and Wang, 1997; Sontag, 1998)). In the case of (19) we have an integral-to-integral property (iiIOSS) with $m(\mathbf{w})$ as a measure of the states, so the "energy" of the states is bounded above by the "energy" of the input and output signals. With $E(\mathbf{w})$ as a measure of the states, we can also find a uniform upper bound (as opposed to an "energy" upper bound) in terms of the input and output signals. That is, system (2)–(5) has the IOSS property, as stated formally in the next theorem.

Theorem 4. For $Re \in (0, 4)$, solutions of system (2)–(5) satisfy

$$E(\mathbf{w}(t)) \leq E(\mathbf{w}(0))\, e^{-c_5 t} + \frac{1}{4c_5} \sup_{[0,t]} \left\{ \int_0^L \int_0^{2\pi} \Delta p^2 d\theta dz \right\} + \frac{c_6}{c_5} \sup_{[0,t]} \left\{ \int_0^L \int_0^{2\pi} v_{r-w}^2 d\theta dz \right\} \tag{20}$$

for all $t \geq 0$ and for arbitrary values of the control v_{r-w}, with

$$c_5 = 2\max\left(\frac{4}{3Re} - 1, \frac{4 - Re}{4 + Re}\right) > 0 \text{ and}$$
$$c_6 = \max\left(\frac{1}{4}, \frac{1}{4} + \frac{5Re - 4}{Re(4 - Re)}\right) > 0.$$

In Theorem 4, the notation $\sup_{[0,t]}$ denotes the essential supremum taken over the finite time interval $[0, t]$. The detectability properties stated in Theorems 3 and 4 indicate that our choice of sensing, Δp, is appropriate.

8. NUMERICAL SIMULATIONS

8.1 *The Computational scheme*

The simulations are performed using a flow solver [2] that is based on a second–order staggered grid discretization, second–order time advancement, and a Poisson equation for pressure, based on a scheme designed by Akselvoll and Moin (1996). The length of the cylinder is $L = 3\pi$ and the radius is $R = 1$. The grid is structured, single-block with cylindrical coordinates. It is uniform and periodic in z and θ with Fourier–modes 64 and 128 respectively, and linearly spaced with ratio $8:1$ in the radial direction in order to achieve high resolution at the wall. The adaptive time step was in the range of 0.06-0.08 with constant CFL number 0.5 and constant 1 volume flux per unit span. The Reynolds number we used was $Re = 2100$ which is slightly higher than the limiting number $Re = 2000$ for nonlinear stability. We ran both the controlled and the uncontrolled case for about 110 time units starting from a statistically steady state flow field with control gain $k = 0.1$ in the controlled case. The initial flow field was obtained from a random perturbation of the parabolic profile over a large time interval using the uncontrolled case.

8.2 *Measuring mixing*

Figure 2 shows that our control results in an approximately 50% increase in the perturbation energy and 92% almost instantaneous increase in the enstrophy. While comparison based on perturbation energy is important as it is the part of the cost functional (13), enstrophy provides us with a measurement that is more closely related to mixing.

The method we use to quantify and visualize mixing is the tracking of dye in the flow. We consider the problem of mixing of a single fluid (or similar fluids) governed by the stretching and folding of material elements. We introduce passive tracer dye along the center of the pipe represented by a set of 100 particles (Figure 3). We trace the position of these particles using a particle–line method (Krasnopolskaya *et al.*, 1999; Ten *et al.*, 1998). The distance between neighboring particles is kept under 0.1 by introducing new particles to halve the distance if necessary to obtain a connected dye surface at all time. As shown in Figure 4, the number of particles, that is, the length of the dye, increases in the controlled case at a much higher rate than in the uncontrolled case. Adding particles is not feasible computationally for an extended period of time. We stopped adding particles when their number reached two million ($t = 4$ in the controlled case and $t = 8$ in the uncontrolled case), but we continued tracing them. Figure 5 shows the distribution of particles inside the pipe. In the controlled case we obtain more uniform particle distribution even for smaller time.

8.3 *Actuator distribution and bandwidth*

Figure 6 shows the instantaneous pressure field in a cross section of the pipe along with the boundary

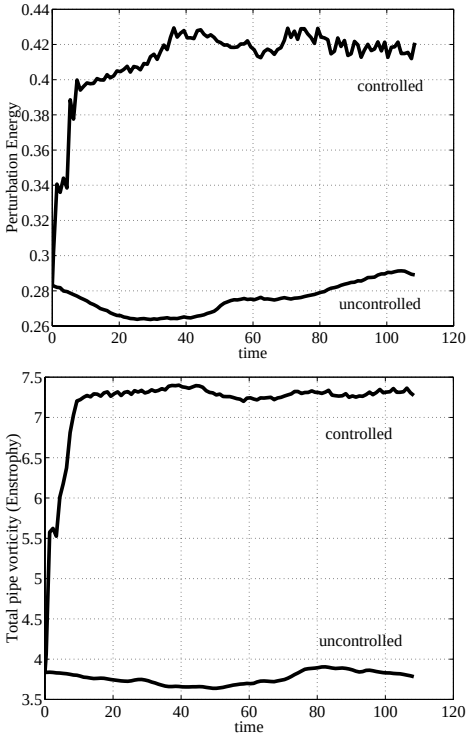

Fig. 2. Perturbation energy and enstrophy.

Fig. 3. Initial particle distribution.

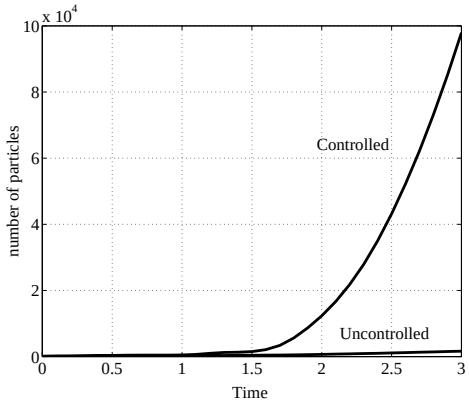

Fig. 4. Length of dye as a function of time.

velocity that is magnified 500 times for visualization. The control "blows in" when wall pressure is high and "sucks out" when wall pressure is low. Spatial changes in the control velocity are smooth and small, promising that low number of actuators will suffice in practice. In order to investigate the density and bandwidth of sensors and actuators needed we calculate the power spectral densities of the control. The spectral plots are shown in Figure 7. Figure 7(a) shows that only about 10-15 actuators/sensors are needed along the pipe length. Similarly, in the angular direction (see Figure 7(b)) we need at most 15-20 actuators/sensors. That re-

[2] We thank Charles Pierce for providing the code for the uncontrolled case.

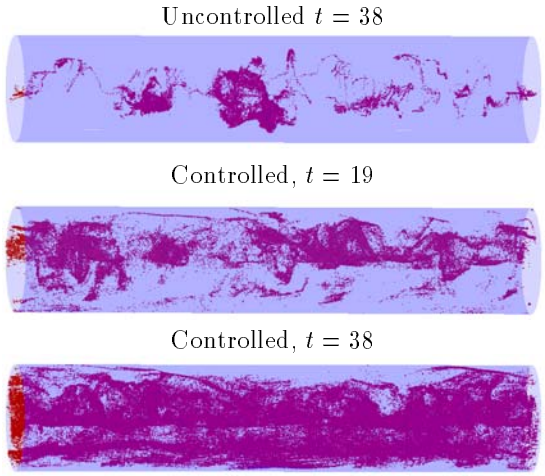

Fig. 5. Particle distribution.

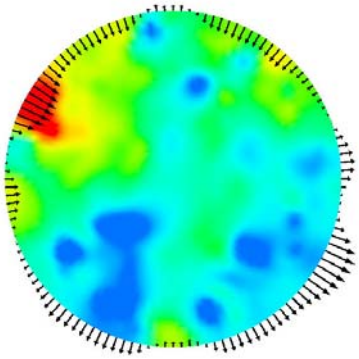

Fig. 6. Instantaneous pressure field with controlled velocity (magnified) in a cross section of the pipe.

sults in approximately 200 micro–actuators/sensors for the whole pipe surface. The time–frequency analysis (Figure 7(c)) shows a bandwidth required for sensing/actuation of only 1.5Hz.

9. REFERENCES

Aamo, O.M., M. Krstić and T.R. Bewley (submitted). Control of mixing by boundary feedback in 2D channel flow.

Akselvoll, K. and P. Moin (1996). An efficient method for temporal integration of the Navier–Stokes equations in confined axisymmetric geometry. *Journal of Computational Physics* **125**, 454–463.

Balogh, A., O.M. Aamo and M. Krstić (submitted). Optimal mixing enhancement in 3D pipe flow.

D'Alessandro, D., M. Dahleh and I. Mezić (1998). Control of fluid mixing using entropy methods. In: *Proceedings of the American Control Conference*. Philadelphia, Pennsylvania.

D'Alessandro, D., M. Dahleh and I. Mezić (1999). Control of mixing in fluid flow: a maximum entropy approach. *IEEE Transactions on Automatic Control* **44**(10), 1852–1863.

Krasnopolskaya, T.S., V.V. Meleshko, G.W.M. Peters and H.E.H. Meier (1999). Mixing in Stokes flow in an annular wedge cavity. *Eur. J. Mech. B/Fluids* **18**, 793–822.

Krichman, M., E.D. Sontag and Y. Wang (2001). Input-output-to-state stability. *SIAM Journal on Control and Optimization* **39**(6), 1874–1928.

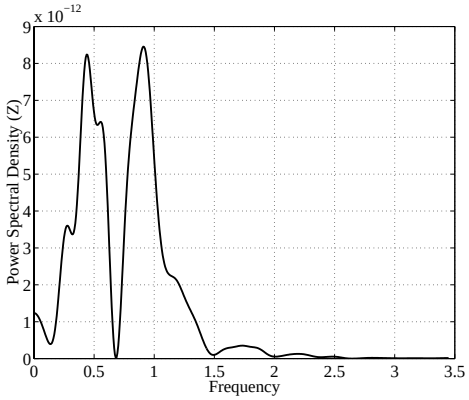

(a) Streamwise direction

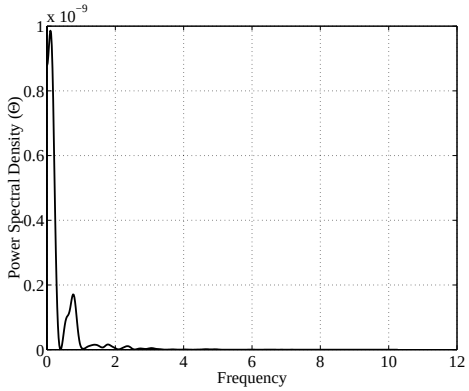

(b) Radial direction

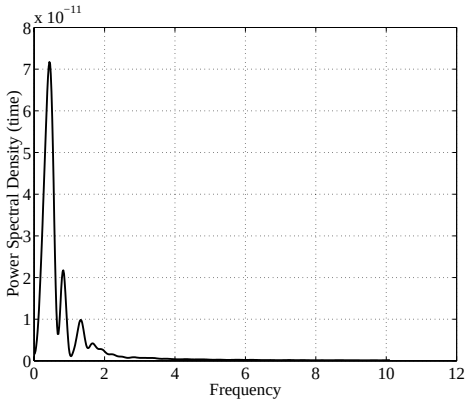

(c) Time

Fig. 7. Spectral analysis of the control.

Mezić, I. (2001). Nonlinear dynamics and ergodic theory methods in control of fluid flows: theory and applications. In: *Proceedings of the 2001 AFOSR Workshop on Dynamics and Control*.

Noack, B.R., I. Mezić and A. Banaszuk (2000). Controlling vortex motion and chaotic advection. In: *Proceedings of the 39th IEEE Conference on Decision and Control*. Sydney, Australia.

Sontag, E.D. (1998). Comments on integral variants of ISS. *Systems & Control Letters* **34**, 93–100.

Sontag, E.D. and Y. Wang (1997). Output-to-state stability and detectability of nonlinear systems. *Systems & Control Letters* **29**, 279–290.

Ten, A.A., Y.Y. Podladchikov, D.A. Yuan, T.B. Larsen and A.V. Malevsky (1998). Comparison of mixing properties in convection with the particle–line method. *Geophys. Res. Lett.* **25**, 3205–3208.